


Effective Floquet Hamiltonians for periodically driven twisted bilayer grapheneMichael Vogl ^{*,†}*Department of Physics, The University of Texas at Austin, Austin, Texas 78712, USA*Martin Rodriguez-Vega ^{*,‡}*Department of Physics, The University of Texas at Austin, Austin, Texas 78712, USA
and Department of Physics, Northeastern University, Boston, Massachusetts 02115, USA*

Gregory A. Fiete

*Department of Physics, Northeastern University, Boston, Massachusetts 02115, USA
and Department of Physics, Massachusetts Institute of Technology, Cambridge, Massachusetts 02139, USA*(Received 25 February 2020; revised manuscript received 10 May 2020; accepted 22 May 2020;
published 5 June 2020)

We derive effective Floquet Hamiltonians for twisted bilayer graphene driven by circularly polarized light in two different regimes beyond the weak-drive, high-frequency regime. First, we consider a driving protocol relevant for experiments with frequencies smaller than the bandwidth and weak amplitudes and derive an effective Hamiltonian, which through a symmetry analysis, provides analytical insight into the rich effects of the drive. We find that circularly polarized light at low frequencies can selectively decrease the strength of AA-type interlayer hopping while leaving the AB-type unaffected. Then, we consider the intermediate frequency and intermediate-strength drive regime. We provide a compact and accurate effective Hamiltonian which we compare with the Van Vleck expansion and demonstrate that it provides a significantly improved representation of the exact quasienergies. Finally, we discuss the effect of the drive on the symmetries, Fermi velocity, and the gap of the Floquet flat bands.

DOI: [10.1103/PhysRevB.101.235411](https://doi.org/10.1103/PhysRevB.101.235411)**I. INTRODUCTION**

The recent discovery of strong-correlation effects in twisted bilayer graphene (TBG) generated great interest in moiré heterostructures [1–31] and ways to simulate them [23]. Similar to the behavior in cuprates [32,33] at different filling factors superconductivity, Mott-insulating [4,16,34–36], and ferromagnetic behavior [37,38] has been observed in TBG. The experimental observations were followed by several theoretical proposals to explain the observations based on the existence of flat bands that appear at special twist angles [1,9,39]. These flat bands play an essential role in the emergence of strong correlations because the interaction terms become relatively dominant [40] over the kinetic energy contributions of the dispersive bands [12,24,36,39–41].

In TBG, the flat bands depend strongly on the twist angle between the graphene layers, which is experimentally difficult to set to a precise value. This challenge has led to several studies proposing different mechanisms to correct for deviations from the magic angle, for example, via pressure [5,42–44] or light confined in a waveguide [45].

In parallel to the developments on moiré lattices, there has been rapid progress in our understanding of nonequilibrium

systems, both experimentally and theoretically, particularly for the case of periodic drives, which may be induced by a laser [46–58]. The existence of an exponentially-long prethermal time regime [59–64] in driven interacting quantum systems allows one to introduce the notion of effective time-independent theories. The development of several techniques to derive effective Hamiltonians in different drive regimes led to rapid evolution of the Floquet engineering field [61,65–86]. For instance, the prediction of an anomalous Hall effect in single-layer graphene driven by circularly polarized light [87] has been recently confirmed in experiments [88]. More generally, there has been an increased interest in the study of topological transitions induced by periodic drives [87,89–107].

More recently, the fields of *twistronics* and Floquet engineering crossed paths in twisted bilayer graphene driven by circularly polarized light in free space [108–110]. Interesting effects like topological transitions at large twist angles using high-frequency drives [108] and the induction of flat bands using near-infrared light in a wide range of twist angles [110] were found. These studies are mainly numerical and only provide analytical descriptions in the high drive frequency regime, which we will define rigorously in the next section.

The aim of this work is to derive analytical effective Floquet Hamiltonians that allow us to gain insight into twisted bilayer graphene subjected to circularly polarized light away from the conventional weak drive, high frequency regime of Van Vleck [111,112], Floquet-Magnus, or Brillouin-Wigner

*These authors contributed equally to this work.

†Corresponding author: ssss133@googlemail.com‡Corresponding author: rodriguezvega@utexas.edu

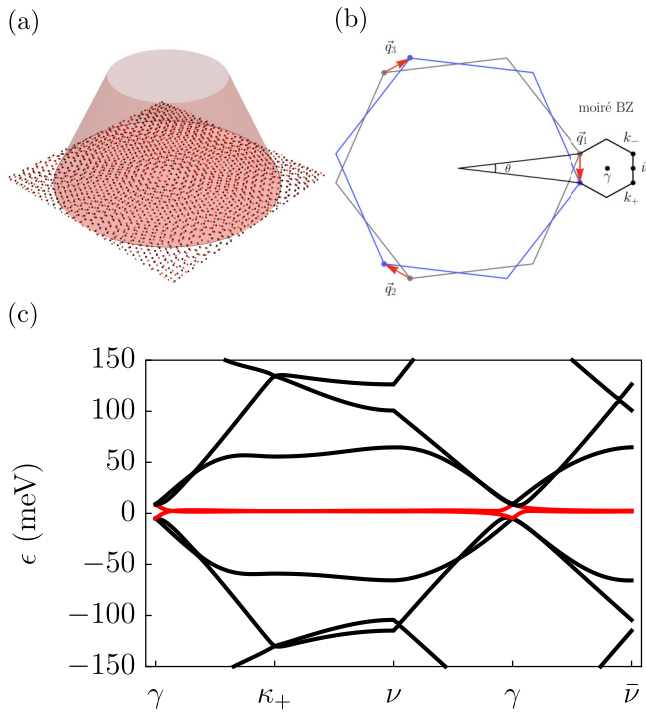


FIG. 1. (a) Sketch of twisted bilayer graphene irradiated by circularly polarized light. (b) Moiré Brillouin zone. (c) Band structure for twisted bilayer graphene for $w_0 = w_1 = 110$ meV and $\theta = 1.05^\circ$. The low-energy flat bands are highlighted in red.

approximations [66,74]. Our effective Floquet Hamiltonians allow us to elucidate the effects of the interplay of moiré lattices and Floquet drives. Particularly, we consider two complementary regimes: (i) a regime characterized by weak drive and low frequencies and (ii) a regime characterized by intermediate frequencies and strong drives. The remainder of the paper is organized as follows: In Sec. II we describe the system we consider, in Sec. III we examine the low-frequency, weak drive limit, and in Sec. IV we address the intermediate frequency and intermediate strength drive regime. Finally, in Sec. V we present our conclusions and outlook.

II. SYSTEM DESCRIPTION

A. Static Hamiltonian

The starting point of our discussion is the effective Hamiltonian that describes twisted bilayer graphene [1,25,39,113–115]

$$H_{\mathbf{k}}(\mathbf{x}) = \begin{pmatrix} h(-\theta/2, \mathbf{k} - \kappa_-) & T(\mathbf{x}) \\ T^\dagger(\mathbf{x}) & h(\theta/2, \mathbf{k} - \kappa_+) \end{pmatrix} \quad (1)$$

which describes two stacked graphene layers that are rotated with respect to each other by an angle θ , as shown in the sketch of Fig. 1(a). Here,

$$h(\theta, \mathbf{k}) = \gamma \begin{pmatrix} 0 & f(R(\theta)\mathbf{k}) \\ f^*(R(\theta)\mathbf{k}) & 0 \end{pmatrix} \quad (2)$$

is the single-layer graphene Hamiltonian, $f(\mathbf{k}) = e^{-\frac{2}{3}ia_0k_y} + 2e^{\frac{ia_0k_y}{3}} \sin(\frac{a_0k_x}{\sqrt{3}} - \frac{\pi}{6})$ describes the intralayer hopping ampli-

tude between nearest-neighbor sites, and $\gamma = v_F/a_0$, where we use natural units $\hbar = c = e = 1$. The inclusion of the full structure of $f(\mathbf{k})$ means that this Hamiltonian is valid in the full Brillouin zone and not just near a K point. The interlayer hopping matrix

$$T(\mathbf{x}) = \sum_{i=-1}^1 e^{-i\mathbf{b}_i \cdot \mathbf{x}} T_i, \quad (3)$$

$$T_n = w_0 \mathbb{1}_2 + w_1 \left(\cos\left(\frac{2\pi n}{3}\right) \sigma_1 + \sin\left(\frac{2\pi n}{3}\right) \sigma_2 \right), \quad (4)$$

describes tunneling between the two graphene layers and encodes a hexagonal pattern that has its origin in that the two superimposed graphene lattices which develop a moiré pattern [see Fig. 1(b)], where $\mathbf{b}_0 = (0, 0)$, and $\mathbf{b}_{\pm 1} = k_\theta (\pm\sqrt{3}/2, 3/2)$ are the reciprocal lattice vectors. Following Refs. [45,109,110] we introduced an additional parameter w_1 into the tunneling term to model relaxation effects, since AB/BA stacking configurations are energetically favored over AA configurations [114,116]. Furthermore, there are indications that AA and AB regions have different interlayer-lattice constants [117]. Throughout this work, we fixed $\gamma = v_F/a_0 = 2.36$ eV, and $a_0 = 2.46$ Å. For a detailed description of the band structure numerical implementation, see the Appendix of Ref. [45]. In Fig. 1(c) we show the band structure for $w_0 = w_1 = 110$ meV, and $\theta = 1.05^\circ$, value near the magic angle.

The Hamiltonian in Eq. (1) describes only one valley degree of freedom. A full description of the system would incorporate the two graphene valleys. However, we only consider perturbations induced by light, which cannot induce processes that mix the two valleys. The Hamiltonian in the other valley is connected by a C_2 rotation [118]. The symmetries of the continuum model Eq. (1) include C_3 rotational symmetry about the center of a AA region, $C_2\mathcal{T}$ symmetry (taking into account both valleys, the TBG presents time-reversal symmetry \mathcal{T}), and $M_y : y, k_y \rightarrow -y, -k_y$ mirror symmetry [16,118,119]. In the small-rotation limit, the angle dependence of the graphene sectors can be neglected, leading to an approximate particle-hole symmetry \mathcal{C} [119].

B. Driven twisted bilayer graphene

For the driven system, we assume that circularly polarized light is applied in a direction normal to the TBG plane as sketched in Fig. 1(a). Then, the light enters via minimal substitution as $k_x \rightarrow \tilde{k}_x(t) = k_x - A \cos(\Omega t)$, and $k_y \rightarrow \tilde{k}_y = k_y - A \sin(\Omega t)$ leaving the tunneling sector almost unaltered. The reason for this is simple. The inclusion of light in a tight-binding model can be done via a Peirls substitution for hoppings $t_{ij} \rightarrow e^{i \int_{R_i}^{R_j} \mathbf{A} d\mathbf{r}} t_{ij}$. The interlayer hopping is dominated by hopping between atoms that are almost exactly on top of each other—after all other atoms are further away and the overlap between orbitals is smaller. Therefore for interlayer couplings mostly longitudinal components of \mathbf{A} contribute in the line integral $\int_{R_i}^{R_j} \mathbf{A} d\mathbf{r}$. Circularly polarized light only has transverse components and therefore has little effect on interlayer couplings. The time-dependent Hamiltonian is

$$H(\mathbf{x}, t) = \begin{pmatrix} h(-\theta/2, \tilde{\mathbf{k}}(t) - \kappa_-) & T(\mathbf{x}) \\ T^\dagger(\mathbf{x}) & h(\theta/2, \tilde{\mathbf{k}}(t) - \kappa_+) \end{pmatrix}, \quad (5)$$

with $H(\mathbf{x}, t + 2\pi/\Omega) = H(\mathbf{x}, t)$. The Floquet theorem [65,66,70] exploits the discrete time-translational symmetry and allows one to write the wave functions as $|\psi(t)\rangle = e^{i\epsilon t}|\phi(t)\rangle$, where $|\phi(t + 2\pi/\Omega)\rangle = |\phi(t)\rangle$ and ϵ is the quasienergy. Replacing $|\psi(t)\rangle$ into the Schrödinger equation leads to $[H(\mathbf{x}, t) - i\partial_t]|\phi(t)\rangle = \epsilon|\phi(t)\rangle$, which governs the dynamics of the periodic system. The exact solution can be generically obtained either by constructing the Floquet evolution operator $U_F = T \exp\{-i \int_0^{2\pi/\Omega} H(s) ds\} = e^{-iH_F T}$

$$f(\mathbf{k}) \rightarrow f^{(n)}(\mathbf{k}) = e^{-\frac{1}{3}i(2a_0k_y + 3(\theta - \pi)n)} \left(1 + 2e^{ia_0k_y} \sin\left(\frac{a_0k_x}{\sqrt{3}} + \frac{2\pi n}{3} - \frac{\pi}{6}\right) \right) J_n\left(\frac{2Aa_0}{3}\right)$$

$$T(\mathbf{x}) \rightarrow T^{(n)}(\mathbf{x}) = \delta_{n,0}T(\mathbf{x}), \quad (6)$$

in Eq. (1).

The two exact approaches outlined above are challenging to use in practice, and one usually has to employ approximations. In the following sections, we will employ a recently developed [79] approach valid in the weak-drive limit and for arbitrary frequencies. Also, we will introduce improved methods to study the intermediate-amplitude drive regime valid in the high and intermediate frequency regimes.

III. WEAK DRIVE REGIME

Thus far, most discussions of twisted bilayer graphene irradiated by circularly polarized light have focused on the high frequency limit. This is for practical reasons because the lower frequency regime, while it is more interesting and relevant for experiments, is also harder to treat using the existing theoretical tools. In Ref. [79], we developed a method to address this issue in the weak driving limit. Here, we apply our method using a series of approximations necessary to make progress and gain some analytical insights into the low frequency regime.

If we are interested in the effects of the drive on the low-energy bands, small angles, and weak drives our original Hamiltonian can be approximated with $f(\mathbf{k}) \approx f_L(\mathbf{k}) = a_0 e^{-i\frac{\theta}{2}}(k_x - ik_y)$, in the vicinity of the graphene K point. The reason we may Taylor expand for small momenta when the twist angle θ is small is because the moiré Brillouin zone is very small, i.e., $k_\theta \ll k_D$. Nonlinear corrections only become important for higher-energy bands. These higher-energy bands are in turn not relevant for the driven system in the weak-drive limit, since they couple weakly to the low-energy bands.

The time-dependent Hamiltonian within these approximations has the form

$$H(t) = H_L + \mathcal{P} e^{-i\Omega t} + \mathcal{P}^\dagger e^{i\Omega t}, \quad (7)$$

where the monochromatic operator $\mathcal{P} = T^{-1} \int_0^T ds H(\mathbf{x}, s) e^{i\Omega s}$ is given by

$$\mathcal{P} = -A\gamma a_0 \begin{pmatrix} 0 & e^{i\theta/2} & 0 & 0 \\ 0 & 0 & 0 & 0 \\ 0 & 0 & 0 & e^{-i\theta/2} \\ 0 & 0 & 0 & 0 \end{pmatrix}, \quad (8)$$

or by employing the extended-state picture. In the extended-state picture, we use the Fourier series $|\phi(t)\rangle = \sum_n e^{in\Omega t} |\phi_n\rangle$, which leads to $\sum_m (H^{(n-m)} + \delta_{n,m}\Omega m) |\phi_m\rangle = \epsilon |\phi_n\rangle$, defined in the infinite-dimensional Floquet-Hilbert space spanned by the direct product of the Hilbert space of the static system and the space spanned by a complete set of periodic functions. The Hamiltonian Fourier modes are given by $H^{(n)} = \int_0^{2\pi} d\tau / (2\pi) H(\tau) e^{-in\tau}$, which can be derived by making the replacements

and H_L is the same as Eq. (1) just with $f(\mathbf{k}) \rightarrow f_L(\mathbf{k})$ linearized momentum dependence.

For weak driving amplitudes A and arbitrary frequency Ω , the periodically driven systems can be described by the effective self-consistent time-independent Hamiltonian [79]

$$H_{\text{eff}} \approx H_L + P \frac{1}{\epsilon - H_L - \Omega} P^\dagger + P^\dagger \frac{1}{\epsilon - H_L + \Omega} P, \quad (9)$$

where H_0 is the time-averaged Hamiltonian, and ϵ are the quasienergies. For large frequency drives, we can apply a Van Vleck expansion and obtain the effective Hamiltonian [111,112] $H_{\text{eff}} = H_L + H_\Omega$, where the leading order correction is given by $H_\Omega = -\Delta\tau_0 \otimes \sigma_3$, $\Delta = (A\gamma a_0)^2/\Omega$, and σ_i , τ_i are the Pauli matrices in pseudo-spin and layer space, respectively. To keep the notation simple, in the remainder of the text we refer to the approximation $H_{\text{eff}} \approx H_L + [P^\dagger, P]$ as the Van Vleck approximation.

Therefore, in the high-frequency limit, the main effect is the addition of the gap Δ in the quasienergy spectrum originating from the breaking of time-reversal symmetry \mathcal{T} . This gap is topologically nontrivial, and leads to topological Floquet flat bands with Chern number $C = 4$ [109,110] which could serve as platforms to realize Floquet fractional Chern insulators [109,120]. The relatively large Chern number originates from spin and valley degeneracy [109,110].

In order to evaluate the effective Hamiltonian H_{eff} for arbitrary frequency, we notice that the Brillouin zone has dimensions $k_\theta \propto \sin(\theta/2)$ and therefore the corresponding energy obeys $\hbar v_F k_\theta \ll w_{0,1}$ for sufficiently low angles. This is, for small angles, $T(\mathbf{x})$ introduces the dominant energy scale, i.e., $\min \|T(\mathbf{x})\| \gg \|h(\mathbf{k})\|$, where $\|\cdot\|$ is a matrix norm. This estimate can be written more precisely as

$$\sqrt{(\mathbf{k} - \kappa_+)^2 + (\mathbf{k} - \kappa_-)^2} \ll 3 \frac{w_1}{\hbar v_F} \quad (10)$$

if $w_0 \approx w_1$. (Physically, this is a regime where the inter-layer coupling are essential to the physics.) Therefore, for small enough angles and momenta that fulfill this inequality we may introduce the approximation $(\epsilon - H_L \pm \Omega)^{-1} \approx (\epsilon - H_T \pm \Omega)^{-1}$ where

$$H_T = \begin{pmatrix} 0 & T(\mathbf{x}) \\ T^\dagger(\mathbf{x}) & 0 \end{pmatrix}. \quad (11)$$

Replacing this approximation in the second and third terms of equation (9), we find the effective Hamiltonian $H_{\text{eff}} = H_0 + H_\Omega + \mathcal{O}((\frac{A}{k_D})^3, (\frac{A}{k_D})^2 \frac{k_D}{k_D})$, where the neglected terms that are third order in small parameters. We find that terms of order $\mathcal{O}(\frac{A}{k_D})^4$ vanish. The leading-order correction to the Hamiltonian H_Ω has the following form

$$\begin{aligned} H_\Omega(\mathbf{x}) = & V(\mathbf{x}, \Omega)\tau_0 \otimes \sigma_0 + U(\mathbf{x}, \Omega)\tau_3 \otimes \sigma_0 \\ & + \frac{1}{2}\Delta_1(\mathbf{x}, \Omega)(\tau_0 + \tau_3) \otimes \sigma_3 \\ & + \frac{1}{2}\Delta_2(\mathbf{x}, \Omega)(\tau_0 - \tau_3) \otimes \sigma_3 \\ & + \delta w_0(\mathbf{x}, \Omega)\tau^+ \otimes \sigma_0 + \delta w_0^*(\mathbf{x}, \Omega)\tau^- \otimes \sigma_0 \\ & + \beta(\mathbf{x}, \Omega)\tau^+ \otimes \sigma_3 + \beta^*(\mathbf{x}, \Omega)\tau^- \otimes \sigma_3. \end{aligned} \quad (12)$$

Equation (12) is the first main result of our work. The full expressions for each of the terms appearing in Eq. (12) are given in Appendix and depend on the quasienergy, which was omitted explicitly for brevity. A perturbative approach generically generates long-range hopping terms as the frequency is arbitrarily decreased. The method here employed leads to the closed form in Eq. (12), which contains all the possible terms that can be generated by the drive, even in the low-frequency regime, defined as driving frequency $\Omega \lesssim W$ with $W \sim \max_t \|H(t)\|$. Conversely, we define the high-frequency regime for the moiré system as $\Omega > W \sim \max_t \|H(t)\|$.

Now, we discuss the origin and implications of each the new terms on the symmetries of the system. Due to the assumed approximations, the corrections to the Hamiltonian $H_\Omega(\mathbf{x})$ present no momentum dependence and do not commute at different points in space, $[H_\Omega(\mathbf{x}), H_\Omega(\mathbf{x}')] \neq 0$.

The first term, $V(\mathbf{x}, \Omega)\sigma_0 \otimes \tau_0$, with $V(\mathbf{x}, \Omega) \propto \mathcal{O}(\Omega^{-2})$, corresponds to an overall position-dependent potential which does not introduce new physics. The second term, $U(\mathbf{x}, \Omega)\sigma_0 \otimes \tau_3$, is a position-dependent interlayer bias with $U(x, y) = U(x, -y)$, $U(x, y) = -U(-x, y)$, and $U(x, y) \propto \mathcal{O}(\Omega^{-3})$. This term breaks mirror symmetry M_y and allows a relative shift in quasienergy between the Dirac crossings at κ_\pm , as shown schematically in Fig. 2(a) for a spatially-uniform constant U . Because the $U(\mathbf{x}, \Omega)$ is odd in the x coordinate, $C_2\mathcal{T}$ and C_3 are also broken when taking the position dependence into account.

In Bernal-stacked bilayer graphene, an interlayer bias U opens up a gap in the energy spectrum around the K points [121,122]. If we introduce a region in space where the sign of the interlayer bias changes, $U \rightarrow -U$, a domain wall forms where the gap inverts, leading to topologically protected helical (TPH) modes [123–125]. In twisted bilayers, even though U does not gap the spectrum, the moiré pattern alternating AB/BA regions leads to the formation of topological boundary modes even for spatially-homogeneous interlayer bias U [126]. Here, we obtained that circularly polarized light induces an interlayer potential $U(\mathbf{x}, \Omega)$ in the low-frequency limit, which could induce the formation of topologically protected helical modes.

Next, the terms $\Delta_{1/2}(\mathbf{x}, \Omega)(\tau_0 \pm \tau_3) \otimes \sigma_3$ with $\Delta_{1/2}(x, -y) = \Delta_{1/2}(x, y)$ and $\Delta_2(x, y) = \Delta_1(-x, y)$ break M_y , and $C_2\mathcal{T}$ symmetry, which protects the linear band crossing, leading to the opening of a gap at the κ_\pm points in the mBZ. The $\Delta_{1/2}(\mathbf{x}, \Omega)$ position dependence is relevant

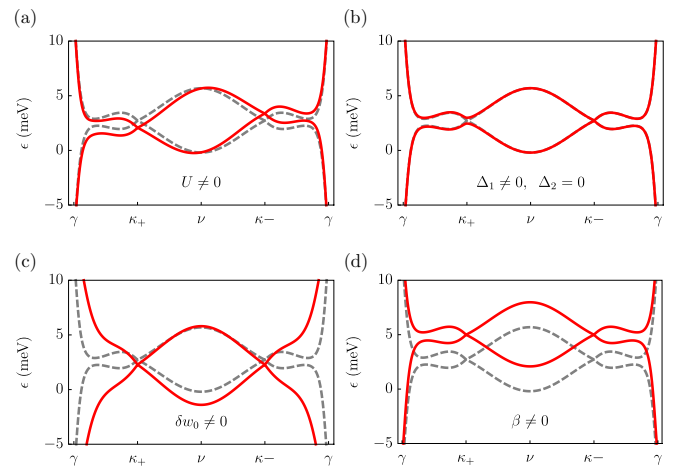


FIG. 2. Sketch of the individual effects of the new term generated by low-frequency and low-intensity circularly polarized light on the TBG quasienergies. The parameters used are $w_0 = w_1 = 110$ meV, and $\theta = 1.2^\circ$. The gray dashed curves correspond to the static case, while the red curve indicates the effect introduced by the nonzero perturbation introduced by light.

at order $\mathcal{O}(\Omega^{-3})$, and the asymmetry $\Delta_1 \neq \Delta_2$ is relevant at order $\mathcal{O}(\Omega^{-4})$. When both TBG valleys are taken into account, this term breaks time-reversal symmetry \mathcal{T} and leads to the formation of topologically nontrivial Floquet flat bands [109,110]. The asymmetry $\Delta_1 \neq \Delta_2$ leads to asymmetric gaps at the κ_\pm points in the mBZ, as sketched in Fig. 2(b), where we plot the bands for TBG with a constant term of the form $\Delta_1(\tau_0 \pm \tau_3) \otimes \sigma_3$ added. The $\Delta_{1/2}(\mathbf{x}, \Omega)$ position dependence leads to breaking of C_3 symmetry.

The term $\delta w_0(\mathbf{x}, \Omega)\tau^+ \otimes \sigma_0$ (and its hermitian conjugate) where $\tau^\pm = 1/2(\tau_1 \pm i\tau_2)$, $\text{Re } \delta w_0(x, -y) = \text{Re } \delta w_0(x, y)$, $\text{Im } \delta w_0(x, -y) = -\text{Im } \delta w_0(x, y)$, $\delta w_0(-x, y) = \delta w_0(x, y)$ introduces a correction to the tunneling amplitude w_0 , consistent with the symmetries of the static system, except C_3 . $\delta w_0(\mathbf{x}, \Omega)$ effectively renormalizes the Fermi velocity at the κ_\pm points and can modify the position of the magic angles. To leading order, $\delta w_0(\mathbf{x}, \Omega) \approx -(A\gamma a_0/\Omega)^2 T_{11}(\mathbf{x}) \cos(\theta)$, where $T_{11}(\mathbf{x}, \Omega)$ corresponds to the diagonal entry of the tunneling matrix Eq. (3).

In Fig. 2(d), we schematically show the effect of this term in the Floquet bands. Controlled drive protocols to tune the Fermi velocity of the Floquet zone center flat quasienergy bands have previously been proposed [45]. For small angles, large drive frequency Ω , and small quasienergies $\epsilon \ll \Omega$, this term constitutes the second most relevant correction after $\Delta_{1/2}(\mathbf{x}, \Omega)$. An accurate description of the quasienergies ϵ near the Floquet zone center is challenging to achieve with high-frequency expansions such as the Magnus expansion, which highlights the strength of our approach. Crucially, the physics of the Floquet bands near the Floquet zone center is not obfuscated by negligible contributions from static high-energy bands which do not hybridize due to the weak drives considered here. Finally, the correction to the interlayer tunneling $\delta w_0(\mathbf{x}, \Omega)$ bears resemblance to effects one would expect from the relaxation of the driven lattice. Particularly, this term only affects the AA-type interlayer coupling w_0 ,

which reduces. One could observe a similar effect if the size of AA-type patches were to shrink, which would also lead to the reduction in w_0 . Secondly if the interlayer distance in AA stacked regions increased, this would also lead to a similar reduction of w_0 . Therefore the periodic drive is able to mimic these effects.

Finally, we address the term $\beta(\mathbf{x}, \Omega)\tau^+ \otimes \sigma_3$ (and its hermitian conjugate) with real-space transformation properties $\beta(-x, y) = \beta(x, y)$, $\text{Re}\beta(x, -y) = \text{Re}\beta(x, y)$, and $\text{Im}\beta(x, -y) = -\text{Im}\beta(x, y)$. To leading order, $\beta(\mathbf{x}, \Omega) = i(A\gamma a_0/\Omega)^2 T_{11}(\mathbf{x}) \sin \theta + O(\Omega^{-3})$. Neglecting its position dependence, β preserves $C_2\mathcal{T}$ and M_y . Taking the position dependence into account, $\beta(\mathbf{x})$ breaks both $C_2\mathcal{T}$ and M_y . Physically $\beta(\mathbf{x}, \Omega)$ can be interpreted as a pseudo-spin dependent tunneling term. Therefore, in the weak-drive, small angle and low-frequency regime, circularly polarized light can introduce a collection of symmetry-breaking processes beyond the reach of the high-frequency limit.

In addition to the small angle limit where Eq. (10) is fulfilled let us also consider the opposite limit

$$\sqrt{(\mathbf{k} - \kappa_+)^2 + (\mathbf{k} - \kappa_-)^2} \gg 3 \frac{w_1}{\hbar v_F} \quad (13)$$

where $(\epsilon - H_L \pm \Omega)^{-1} \approx (\epsilon - H_g \pm \Omega)^{-1}$ with

$$H_g = \begin{pmatrix} h(-\theta/2, \mathbf{k} - \kappa_-) & 0 \\ 0 & h(\theta/2, \mathbf{k} - \kappa_+) \end{pmatrix}. \quad (14)$$

In this case we find that $H_{\text{eff}} = H_0 + H_\Omega + O((\frac{A}{k_D})^3, (\frac{A}{k_D})^2 \frac{w_{1,2}}{\gamma})$

$$\begin{aligned} H_\Omega(\mathbf{k}) &= V(\mathbf{k}, \Omega)\tau_0 \otimes \sigma_0 + U(\mathbf{k}, \Omega)\tau_3 \otimes \sigma_0 \\ &+ \frac{1}{2}\Delta_1(\mathbf{k}, \Omega)(\tau_0 + \tau_3) \otimes \sigma_3 \\ &+ \frac{1}{2}\Delta_2(\mathbf{k}, \Omega)(\tau_0 - \tau_3) \otimes \sigma_3. \end{aligned} \quad (15)$$

The gaps are given as

$$\frac{\Delta_{1/2}(\mathbf{k}, \Omega)}{A^2 a_0^2 \gamma^2} = \frac{\Omega(\epsilon^2 - \Omega^2 + |f_{1/2}(\mathbf{k})|^2)}{\Lambda_{1/2}(\epsilon, \mathbf{k}, \Omega)}, \quad (16)$$

the interlayer bias is

$$\frac{U(\mathbf{k}, \Omega)}{A^2 a_0^2 \gamma^2} = -\frac{\epsilon}{2} \sum_{m=1}^2 (-1)^m \frac{\epsilon^2 - \Omega^2 - |f_m(\mathbf{k})|^2}{\Lambda_m(\epsilon, \mathbf{k}, \Omega)}, \quad (17)$$

and

$$\frac{V(\mathbf{k}, \Omega)}{A^2 a_0^2 \gamma^2} = \frac{\epsilon}{2} \sum_{m=1}^2 \frac{\epsilon^2 - \Omega^2 - |f_m(\mathbf{k})|^2}{\Lambda_m(\epsilon, \mathbf{k}, \Omega)}, \quad (18)$$

where $f_{1/2}(\mathbf{k}) = f(R(\mp\theta/2)(\mathbf{k} - \kappa_\mp))$, with the property $|f_{1/2}(k_x, -k_y)|^2 = |f_{2/1}(\mathbf{k})|^2$, and

$$\Lambda_{1/2}(\epsilon, \mathbf{k}, \Omega) = \prod_{m=1}^2 (|f_{1/2}(\mathbf{k})|^2 - (\epsilon + (-1)^m \Omega)^2), \quad (19)$$

with $\Lambda_{1/2}(\epsilon, (k_x, -k_y), \Omega) = \Lambda_{2/1}(\epsilon, \mathbf{k}, \Omega)$. This property implies that $V((k_x, -k_y), \Omega) = V(\mathbf{k}, \Omega)$, $U((k_x, -k_y), \Omega) = -U(\mathbf{k}, \Omega)$, and $\Delta_{1/2}((k_x, -k_y), \Omega) = \Delta_{2/1}(\mathbf{k}, \Omega)$. Furthermore, $U(\mathbf{k}, \Omega)$, $V(\mathbf{k}, \Omega)$, and $\Delta_{1/2}(\mathbf{k}, \Omega)$ are invariant under a C_3 rotation of the momentum, since $|f_{1/2}(C_3\{\mathbf{k}\})|^2 = |f_{1/2}(\mathbf{k})|^2$. We find that not all terms appearing in Eq. (12)

TABLE I. This table lists the symmetries that are broken for the different terms that can be generated for the case of position dependence, momentum dependence, or if the term is constant. A check mark means that the symmetry is preserved, while a cross means that symmetry is broken.

	$C_2\mathcal{T}$	C_3	M_y
U	✓	✓	x
$U(\mathbf{x})$	x	x	x
$U(\mathbf{k})$	✓	✓	✓
Δ	x	✓	x
$\Delta(\mathbf{x})$	x	x	x
$\Delta(\mathbf{k})$	x	✓	x
$\delta\omega_0$	✓	x	✓
$\delta\omega_0(\mathbf{x})$	✓	x	✓
β	✓	x	✓
$\beta(\mathbf{x})$	x	x	x

valid in the limit Eq. (10) are generated and that they are momentum dependent rather than position dependent. A summary of the results for what symmetries get broken by the different terms is given in Table I.

The more general case, where neither condition Eq. (10) nor the opposite Eq. (13) are fulfilled, we can use the general form of \mathcal{P} to find that an effective Hamiltonian has the same structure as Eq. (12). However, all terms have an additional momentum dependence (e.g., $\Delta_{1,2}(\mathbf{x}, \Omega) \rightarrow \Delta_{1,2}(\mathbf{x}, \mathbf{k}, \Omega)$ etc.). While it is possible to determine that H_Ω has this structure generally, the coefficients are too cumbersome to compute and are therefore not discussed.

IV. INTERMEDIATE DRIVE REGIME

A. Issues with the usual form of the rotating frame transformation

A standard approach for treating systems subjected to intermediately strong drives and intermediate frequencies is applying a rotating frame transformation before the use of a high frequency Magnus expansion [70,77,78]. To accomplish when a Hamiltonian has the form $H(t) = H_0 + \lambda V(t)$, one applies the unitary transformation $U(t) = e^{-i\lambda \int dt V(t)}$ to remove $V(t)$ to lowest order. A large term $\lambda V(t)$ in the Hamiltonian can be traded this way for strongly oscillating terms [70]. This approach allows treating regimes where λ is too large for a Magnus approximation to be applicable and is known to give results that are more reliable than the Magnus expansion [70,77,78].

First, we consider the simpler driven Dirac model

$$H_D = \begin{pmatrix} 0 & k_x - ik_y + \lambda e^{-i\Omega t} \\ k_x + ik_y + \lambda e^{i\Omega t} & 0 \end{pmatrix}, \quad (20)$$

which also describes the upper layer of twisted bilayer graphene near the K point for $w_1 = w_0 = 0$, $\gamma = a_0 = 1$, $\kappa_\pm = 0$ and very small θ . Application of the unitary transformation $U(t) = e^{-i\lambda \int dt V(t)}$ followed by a zeroth order Magnus approximation leads to a Hamiltonian of the form

$$H_{\text{eff,D}} = (\mathbf{B} + R_y(\tau)(\kappa_1, \kappa_2, 0)^T) \cdot \sigma, \quad (21)$$

where $R_y(\tau)$ is a rotation matrix around the y axis by an angle

$$\tau = \tan^{-1} \left(\frac{sJ_1(s)}{sJ_0(s) - J_1(s) + \frac{s}{2}} \right), \quad (22)$$

$s = \frac{4\lambda}{\Omega}$, and $J_n(x)$ is the n th Bessel function of the first kind. The Hamiltonian has a constant fieldlike part with

$$B_x = \frac{\lambda}{2} - \lambda \left(J_0(s) - \frac{J_1(s)}{s} \right), \quad (23)$$

$$B_y = 0, \quad (24)$$

$$B_z = \frac{1}{s} \lambda (J_0(s) - 1) - \lambda J_1(s), \quad (25)$$

and momenta given by

$$\bar{k}_x = k_x(s + 2sJ_0(s) - 2J_1(s)) \times \frac{\sqrt{\frac{2s^2 J_0(s)(1-2J_2(s)) + s^2(1-2J_2(s)) + 4(s^2+1)J_1(s)^2}{(s+2sJ_0(s)-2J_1(s))^2}}}{2s}, \quad (26)$$

$$\bar{k}_y = \frac{1}{2} k_y \left(\frac{2J_1(s)}{s} + 1 \right). \quad (27)$$

By inspecting \bar{k}_x and \bar{k}_y , we realize that k_x and k_y are not treated on equal grounds in this approximation. Specifically, the Fermi velocity has become anisotropic. The quasienergy spectrum is not rotationally symmetric for large driving λ . Specifically if we expand $\bar{k}_{x,y} \approx k_{x,y} \left(1 - \frac{s^2}{16} \mp \frac{s^4}{384} \right)$ we see that the anisotropic behavior appears at fourth order in s that is for relatively large λ . This is in qualitative disagreement with exact numerical calculations, which present rotationally-symmetric quasienergies. Since the problem already appears in the Dirac case, we can therefore expect the rotating frame approximation to also produce unphysical artifacts for the more complicated problem of twisted bilayer graphene. It is important to note that the same type of unphysical anisotropy already appears on the level of a first order Magnus expansion [65]. Therefore, a more careful partial resummation of the Magnus expansion is needed.

B. A better choice of unitary transformation

In order to avoid introducing unphysical terms in the effective Floquet Hamiltonian, we write the time-dependent Hamiltonian as $H(t) = H_0 + \lambda V_1(t) + \lambda V_2(t)$ with $[V_i(t), V_j(t_1)] = 0$ and apply the modified unitary transformation $U(t) = e^{-i \int dt V_1(t)} e^{-i \int dt V_2(t)}$ with $V_1(t) = \lambda \cos(\Omega t) \sigma_1$ and $V_2(t) = \lambda \sin(\Omega t) \sigma_2$. There is an associated arbitrariness in the exact form of this unitary transformation arising from the choice of V_1 and V_2 . However, given our implicit Floquet gauge choice $t^* = 0$, in a time-ordered exponential that removes all of $V_1 + V_2$ we make the smaller error by removing a V_1 first, that is the larger of the two at $t^* = 0$. In the Dirac model this choice can be justified even better *a posteriori* by realizing that it restores the rotational invariance in momentum space. We will make an analogous choice of unitary transformations for the TBG case in Sec. IV D, where we will explicitly demonstrate that the anisotropy in the Fermi velocity is not present.

C. Improved Van Vleck approximation

In this section, we identify a procedure to improve the Van Vleck expansion used to obtain an effective Floquet Hamiltonian which we will use as a baseline to compare our improved rotating frame effective Hamiltonian. For small twist angles θ it is sensible to treat \mathbf{k} as a small parameter because the dimensions of the moiré Brillouin zone are proportional to $\sin(\theta/2)$. Therefore, we may approximate $f(\mathbf{k} - \mathbf{A}) \approx f(-\mathbf{A}) + (k_x(\partial_{k_x} f)(-\mathbf{A}) + k_y(\partial_{k_y} f)(-\mathbf{A}))$. In the weak-strength drive regime, $A \ll a_0$, we employed a simple Taylor expansion. However, in order to capture the effect of stronger drives, we need to improve our approach. For this, we perform a Fourier series in terms of $e^{i\Omega t}$ instead. The result to first order in Fourier components has the form $f(\mathbf{k} - \mathbf{A}) \approx a_0(k_x - ik_y)J_0(2a_0A/3) - 3J_1(2a_0A/3)e^{i\Omega t} - a_0(k_x + ik_y)J_1(2a_0A/3)e^{-i\Omega t}$. For $2a_0A/3$ not too large compared with unit, $J_1(2a_0A/3) \ll 1$. Therefore, terms like $k_i J_1(2a_0A/3)$ are higher order and can be neglected. We will thus work with the approximation

$$f(\mathbf{k} - \mathbf{A}) \approx a_0(k_x - ik_y)J_0\left(\frac{2a_0A}{3}\right) - 3J_1\left(\frac{2a_0A}{3}\right)e^{i\Omega t}. \quad (28)$$

This type of approximation is reasonable for small angles and $2a_0A/3 \lesssim 1$.

After application of this approximation we can readily improve on the Van Vleck approximation, which we will use to compare our results from the rotating wave approximation. The effective Floquet Hamiltonian keeps the same structure as previously obtained, $H_{\text{eff}}^{\text{VV}} = H_L - \Delta \tau_0 \otimes \sigma_3$ with gap

$$\Delta = \frac{9\gamma^2}{\Omega} J_1\left(\frac{2Aa_0}{3}\right)^2 \quad (29)$$

and a renormalized Fermi velocity

$$\tilde{v}_F = v_F J_0\left(\frac{2Aa_0}{3}\right). \quad (30)$$

D. Rotating frame Hamiltonian

In this section, we will derive an effective Floquet Hamiltonian using a rotating frame approach, H_{eff}^R , with an improved unitary transformation. Then, we compare the quasienergies obtained with the ones derived from the Van Vleck Hamiltonian $H_{\text{eff}}^{\text{VV}}$.

We write the time-dependent Hamiltonian for twisted bilayer graphene as $H(t) = H_L + V_1(t) + V_2(t)$, where the time dependent potentials are given as

$$V_1(t) = -3J_1(2a_0A/3) \cos(\Omega t) \begin{pmatrix} \sigma_1^{(-\theta/2)} & 0 \\ 0 & \sigma_1^{(\theta/2)} \end{pmatrix} \quad (31)$$

$$V_2(t) = -3J_1(2a_0A/3) \sin(\Omega t) \begin{pmatrix} \sigma_2^{(-\theta/2)} & 0 \\ 0 & \sigma_2^{(\theta/2)} \end{pmatrix}, \quad (32)$$

where $\sigma_i^\theta = e^{-i\frac{\theta}{2}\sigma_3} \sigma_i e^{i\frac{\theta}{2}\sigma_3}$. After applying the unitary transformation $U(t) = e^{-i \int dt V_1(t)} e^{-i \int dt V_2(t)}$ and after taking an

average over one period $2\pi/\Omega$ we find the following effective Hamiltonian for twisted bilayer graphene that is subjected to circularly polarized light

$$H_{\text{eff}}^R = R \begin{pmatrix} (e^{-i\frac{\theta}{2}} \tilde{v}_F(\mathbf{k} - \kappa_-) + \Delta \hat{e}_z) \cdot \boldsymbol{\sigma} & \tilde{T}(\mathbf{r}) \\ \tilde{T}^\dagger(\mathbf{r}) & (e^{i\frac{\theta}{2}} \tilde{v}_F(\mathbf{k} - \kappa_+) + \Delta \hat{e}_z) \cdot \boldsymbol{\sigma} \end{pmatrix} R^\dagger, \quad (33)$$

where \hat{e}_z is a unit vector in z direction and $\boldsymbol{\sigma}$ is a vector of Pauli matrices. The unitary transformation

$$R = \begin{pmatrix} e^{\frac{3\gamma J_1(\frac{2Aa_0}{3})}{\Omega} i\sigma_2^{(\theta/2)}} & 0 \\ 0 & e^{\frac{3\gamma J_1(\frac{2Aa_0}{3})}{\Omega} i\sigma_2^{(-\theta/2)}} \end{pmatrix} \quad (34)$$

allows us to cast the Hamiltonian in more readable form. From this unitary transformation, one can directly identify the origin of the spurious anisotropy in momentum that one would find in a Magnus expansion approach. Particularly, an expansion of R for large frequencies unavoidably leads to such an issue.

We find that the Fermi velocity has been renormalized to

$$\tilde{v}_F = v_F J_0\left(\frac{2Aa_0}{3}\right) J_0\left(\frac{6\gamma J_1(\frac{2Aa_0}{3})}{\Omega}\right). \quad (35)$$

In Fig. 3, we show a plot of the Fermi velocity and compare it with the Fermi velocity from the improved Van Vleck approximation $H_{\text{eff}}^{\text{VV}}$. We find that the renormalization of the Fermi velocity is $\sim 10\%$ in some regions even for relatively high frequencies.

Furthermore, in H_{eff}^R , the quasienergy gap that is renormalized to

$$\tilde{\Delta} = \frac{3}{\sqrt{2}} \gamma J_1\left(\frac{2Aa_0}{3}\right) J_1\left(\frac{6\sqrt{2}\gamma J_1(\frac{2Aa_0}{3})}{\Omega}\right). \quad (36)$$

A comparison with the Van Vleck result is shown in Fig. 4. We find that also in this case there is considerable difference ($\sim 10\%$ in some regions in parameter space) even for relatively large driving frequencies $\Omega = 2\gamma$. The most striking difference between $H_{\text{eff}}^{\text{VV}}$ and H_{eff}^R appears in the tunneling sector,

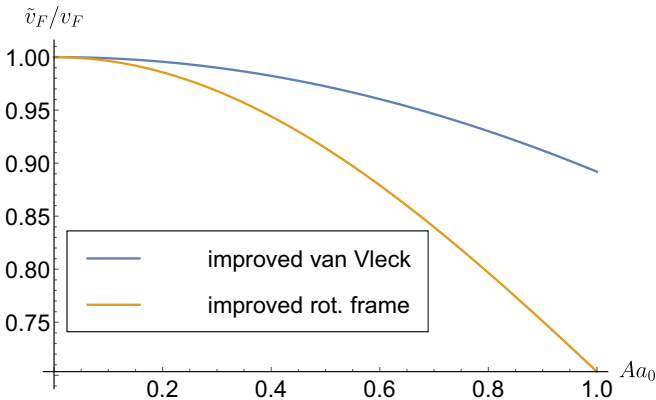


FIG. 3. Fermi velocity normalized to bare v_F for relatively high frequency drives $\frac{\gamma}{\Omega} = \frac{1}{2}$. In blue, we show the Van Vleck result and in orange the renormalized result employing our improved rotating frame approximation.

where H_{eff}^R contains renormalized interlayer hopping

$$\tilde{T}(\mathbf{x}) = \sum_{l=-1}^1 e^{-i\mathbf{b}_l \cdot \mathbf{x}} (\tilde{T}_l - i\beta \sigma_3) \\ \tilde{T}_n = \tilde{w}_0 \mathbb{1}_2 + \tilde{w}_1 \left(\cos\left(\frac{2\pi n}{3}\right) \sigma_1 + \sin\left(\frac{2\pi n}{3}\right) \sigma_2 \right), \quad (37)$$

with

$$\tilde{w}_1 = w_1 J_0\left(\frac{6\gamma J_1(\frac{2Aa_0}{3})}{\Omega}\right) \quad (38)$$

$$\tilde{w}_0 = w_0 \left[1 + \sin^2\left(\frac{\theta}{2}\right) \left(J_0\left(\frac{6\sqrt{2}\gamma J_1(\frac{2Aa_0}{3})}{\Omega}\right) - 1 \right) \right], \quad (39)$$

and a new imaginary term in the AA interlayer coupling

$$\beta = \frac{1}{2} \sin(\theta) \left(1 - J_0\left(\frac{6\sqrt{2}\gamma J_1(\frac{2Aa_0}{3})}{\omega}\right) \right). \quad (40)$$

In the notation of the previous Sec. III the new coupling term enters as $-i\beta \tau^+ \otimes \sigma_3$ and is position dependent. The new dynamically-generated tunneling component β breaks C_3 , the approximate particle-hole symmetry \mathcal{C} , $C_2\mathcal{T}$ and reflection M_y symmetries.

In Fig. 5, we compare our results using H_{eff}^R in Eq. (33) to exact numeric results obtained from an extended space approach [65]. We use the improved Van Vleck approximation $H_{\text{eff}}^{\text{VV}} = H_L - \Delta \tau_0 \otimes \sigma_3$ as a benchmark. We find that the Van Vleck approximation is only valid until $a_0 A \approx 0.4$, while the new approximation works well until $a_0 A \approx 0.8$. The approximation therefore has double the range of validity and therefore is more reliable.

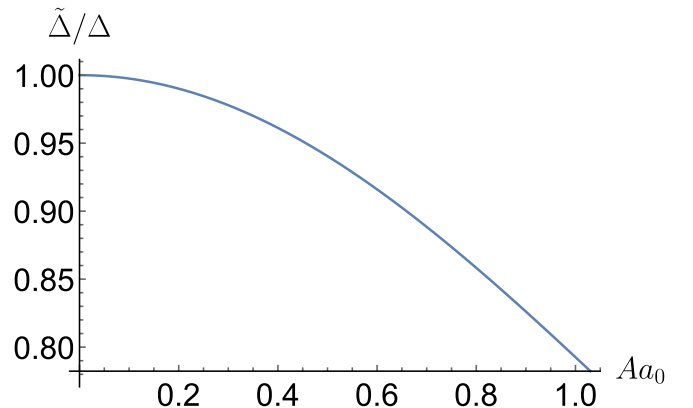


FIG. 4. Ratio $\tilde{\Delta}/\Delta$ of the renormalized gap $\tilde{\Delta}$ and the gap from the Van Vleck Δ for driving frequency $\Omega = 2\gamma$.

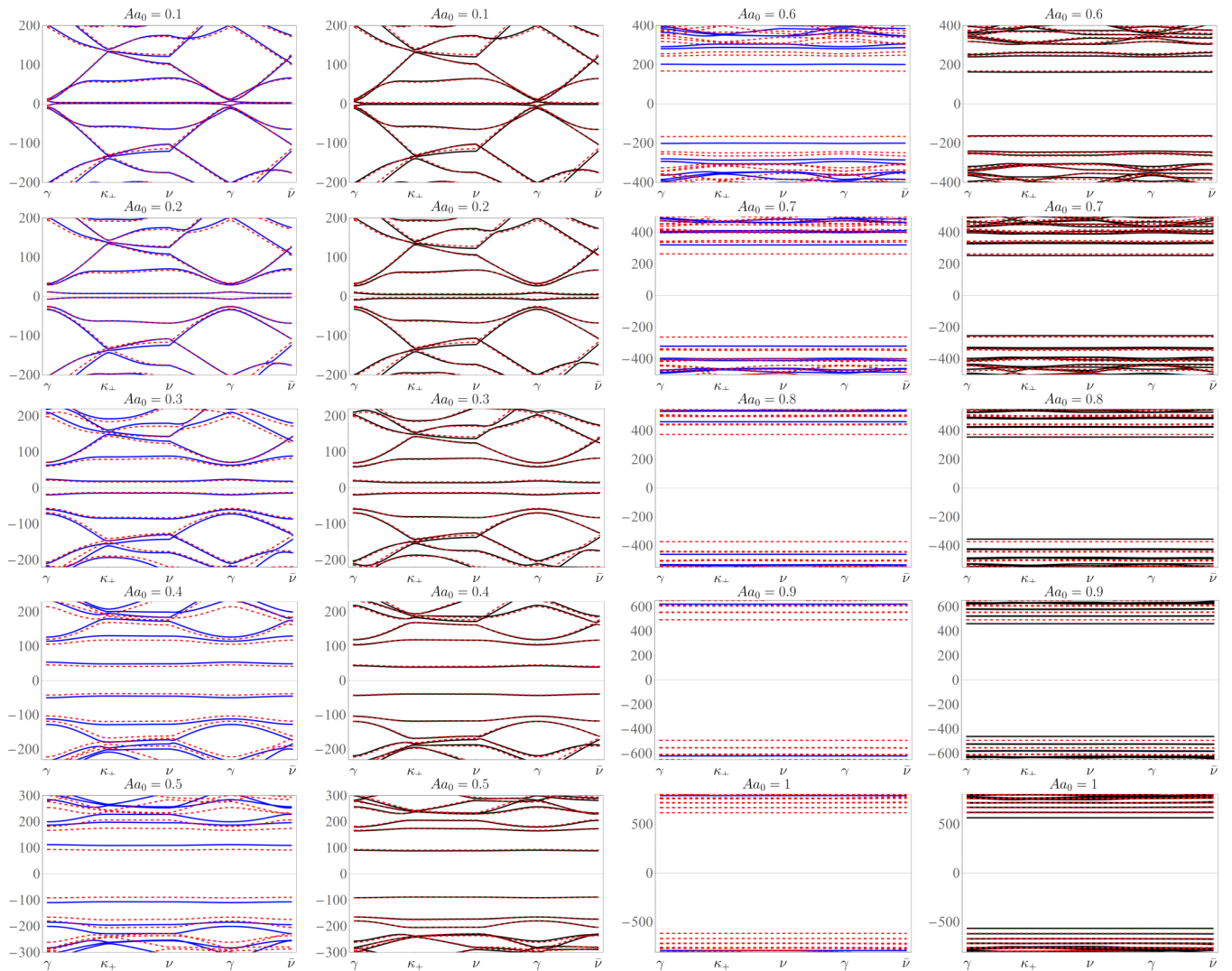


FIG. 5. Quasienergy band structure. The dashed red curves correspond to the exact result, in blue the improved Van Vleck approximation and in black the rotation frame transformation. The parameters used are $\Omega = 2\gamma$, $w_1 = w_0 = 110$ meV, $\gamma = 2364$ meV, and $\theta = 1.05^\circ$.

The same observation can be made a bit more lucidly—albeit losing much information—if we compute the relative error of the gap at the K point $(g_{\text{exact}} - g_{\text{approx}})/g_{\text{exact}}$, where g_{exact} is the “exact” numerical gap at the K point and g_{approx} is the gap for an approximation. For both approximations the result is shown in Fig. 6 below. It is clear from both plots that the rotating frame approximation derived in this paper is far more reliable than the Van Vleck approximation.

V. CONCLUSION AND OUTLOOK

We have introduced two new effective Floquet Hamiltonians that describe twisted bilayer graphene under the influence of circularly polarized light. The Hamiltonians are applicable in the regimes where the ordinary Van Vleck approximation fails. We found that the weak drive strength Hamiltonian, valid even in the low-frequency regime, gives insight into which new terms a periodic drive can generate well beyond the regime of validity of any other approximation scheme. The usefulness of these schemes is limited by the challenge

imposed by the complexity of the terms derived and the self-consistent nature of the low-frequency regime. An important physical effect of the drive in this regime is a renormalization of the interlayer coupling of the AA type. This makes it possible to mimic the effects of some otherwise difficult to achieve structural reorganizations—for instance a change in the distance between the two graphene layers that only appears in AA regions.

The rotating frame Hamiltonian, valid for strong drives and intermediate drive frequencies, reveals that the gap at the Floquet zone center, the Fermi velocity, and the interlayer-coupling strengths are renormalized. This effective Hamiltonian is useful for numerical implementation of the quasienergy band structure and possesses a wide range of validity. This would make it useful for applications where an extended space calculation may be too expensive. For instance if one studies the effect of disorder additional disorder averages make calculations expensive and therefore it might be more feasible to do these calculations using the effective Hamiltonian we presented rather than resorting to a full treatment in an extended space picture.

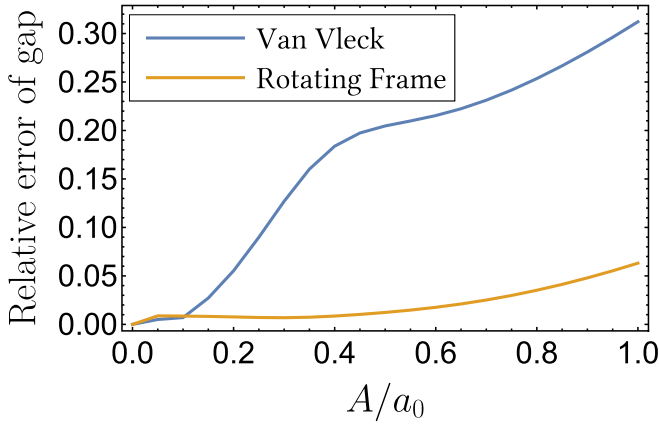


FIG. 6. Plot of the relative error for the gap at the K point of the moiré Brillouin zone. In blue we present our results from the Van Vleck approximation and in orange the results from our improved rotating frame approximation.

ACKNOWLEDGMENTS

We thank Fengcheng Wu for useful discussions. This research was primarily supported by the National Science Foundation through the Center for Dynamics and Control of Materials: an NSF MRSEC under Cooperative Agreement No. DMR-1720595. Partial support was from NSF Grant No. DMR-1949701.

APPENDIX: THE LOW FREQUENCY HAMILTONIAN

The precise form of the effective low frequency Hamiltonian is given as

$$H_{\text{eff}} = H_0 + H_\Omega + \mathcal{O}\left(\left(\frac{A}{k_D}\right)^4, \left(\frac{A}{k_D}\right)^2 \frac{k_\theta}{k_D}\right)$$

$$H_\Omega = A^2 \gamma^2 a_0^2 \begin{pmatrix} W_1^- & 0 & F_- & 0 \\ 0 & W_2^+ & 0 & F_+ \\ F_-^* & 0 & W_2^- & 0 \\ 0 & F_+^* & 0 & W_1^+ \end{pmatrix},$$

$$F_\pm = \frac{e^{\mp i\theta} ((\epsilon \pm \Omega)^2 T_{11}(\mathbf{x}) - \det(T(\mathbf{x})) T_{11}^*(\mathbf{x}))}{D(\epsilon \pm \Omega)},$$

$$W_n^\pm = -\frac{(\epsilon \pm \Omega)[(\epsilon \pm \Omega)^2 - w_0^2 \lambda - w_1^2 \tau_n]}{D(\epsilon \pm \Omega)},$$

$$\lambda = 1 + 4 \cos\left(\frac{\sqrt{3}x_1^\theta}{2}\right) \left(\cos\left(\frac{\sqrt{3}x_1^\theta}{2}\right) + \cos\left(\frac{3x_2^\theta}{2}\right)\right),$$

$$\tau_n = 3 - 4 \cos\left(\frac{3x_2^\theta}{2}\right) \sin\left(\frac{\pi}{6} - \frac{\sqrt{3}}{2}(-1)^n x_1^\theta\right),$$

$$-2 \sin\left((-1)^n \sqrt{3}x_1^\theta + \frac{\pi}{6}\right); \quad x_i^\theta = x_i k_\theta,$$

$$D(\epsilon) = -\epsilon^4 + \epsilon^2 \text{Tr}(T^\dagger(\mathbf{x})T(\mathbf{x})) - |\det T|^2. \quad (\text{A1})$$

The quantities in the main text can be derived from here. We find that the intralayer gaps are given as $\Delta_1(\mathbf{x}) = \frac{1}{2}(W_1^- - W_2^+)$, $\Delta_2(\mathbf{x}) = \frac{1}{2}(W_2^- - W_1^+)$. A Taylor series reveals

$$\frac{\Delta_n(\mathbf{x})}{A^2 \gamma^2 a_0^2} = -\frac{1}{\Omega} - \frac{\epsilon^2 + \text{Tr}(T^\dagger T) - w_0^2 \lambda - w_1^2 \frac{\tau_1 + \tau_2}{2}}{\Omega^3} - (-1)^n \frac{3\epsilon w_1^2 (\tau_1 - \tau_2)}{2\Omega^4} + \mathcal{O}(\Omega^{-5}). \quad (\text{A2})$$

The interlayer bias is given as $U(\mathbf{x}) = \frac{1}{4}(W_1^- - W_1^+ - W_2^- + W_2^+)$. A series expansion is

$$\frac{U(\mathbf{x})}{A^2 \gamma^2 a_0^2} = \frac{(\tau_1 - \tau_2)w_1^2}{2\Omega^3} + \mathcal{O}(\Omega^{-5}). \quad (\text{A3})$$

As last term from the diagonal block we find the overall potential of form $V(\mathbf{x}) = \frac{1}{4}(W_1^- + W_1^+ + W_2^- + W_2^+)$, which is expanded as

$$\frac{V(\mathbf{x})}{A^2 \gamma^2 a_0^2} - \mathcal{O}(\Omega^{-5}) = -\frac{\epsilon}{\Omega^2} - \frac{\epsilon(2\epsilon^2 + 6(\text{Tr}(T^\dagger T) - \lambda w_0^2) - 3w_1^2(\tau_1 + \tau_2))}{2\Omega^4}. \quad (\text{A4})$$

Notably the lowest order term is just a constant shift in quasienergy.

On the off-diagonal blocks we find the interlayer hopping strength $\delta w_0(\mathbf{x}) = \frac{1}{2}(F_- + F_+)$, which to lower order in Ω^{-1} is

$$\frac{\delta w_0(\mathbf{x})}{A^2 \gamma^2 a_0^2} - \mathcal{O}(\Omega^{-5}) = -\frac{T_{11} \cos(\theta)}{\Omega^2} - \frac{2i\epsilon T_{11} \sin(\theta)}{\Omega^3} - \frac{\cos(\theta)(T_{11}(3\epsilon^2 + \text{tr}(T^\dagger T)) - T_{11}^* \det(T))}{\Omega^4}. \quad (\text{A5})$$

Furthermore we find that the interlayer hopping has a bias $\beta = \frac{1}{2}(F_- - F_+)$, which to low orders has the form

$$\frac{\beta(\mathbf{x})}{A^2 \gamma^2 a_0^2} - \mathcal{O}(\Omega^{-5}) = -\frac{iT_{11} \sin(\theta)}{\Omega^2} - \frac{2T_{11}\epsilon \cos(\theta)}{\Omega^3} - \frac{i \sin(\theta)(T_{11}(3\epsilon^2 + \text{Tr}(T^\dagger T)) - T_{11}^* \det(T))}{\Omega^4}. \quad (\text{A6})$$

[1] F. Wu, A. H. MacDonald, and I. Martin, Theory of Phonon-Mediated Superconductivity in Twisted Bilayer Graphene, *Phys. Rev. Lett.* **121**, 257001 (2018).

[2] Y. Cao, V. Fatemi, S. Fang, K. Watanabe, T. Taniguchi, E. Kaxiras, and P. Jarillo-Herrero, Unconventional superconductivity in magic-angle graphene superlattices, *Nature (London)* **556**, 43 (2018).

- [3] K.-T. Tsai, X. Zhang, Z. Zhu, Y. Luo, S. Carr, M. Lusk, E. Kaxiras, and K. Wang, Correlated superconducting and insulating states in twisted trilayer graphene Moiré of Moiré superlattices, [arXiv:1912.03375](#).
- [4] E. Codecido, Q. Wang, R. Koester, S. Che, H. Tian, R. Lv, S. Tran, K. Watanabe, T. Taniguchi, F. Zhang, M. Bockrath, and C. N. Lau, Correlated insulating and superconducting states in twisted bilayer graphene below the magic angle, *Sci. Adv.* **5**, eaaw9770 (2019).
- [5] M. Yankowitz, S. Chen, H. Polshyn, Y. Zhang, K. Watanabe, T. Taniguchi, D. Graf, A. F. Young, and C. R. Dean, Tuning superconductivity in twisted bilayer graphene, *Science* **363**, 1059 (2019).
- [6] D. V. Chichinadze, L. Classen, and A. V. Chubukov, Nematic superconductivity in twisted bilayer graphene, [arXiv:1910.07379](#).
- [7] Y.-Z. Chou, Y.-P. Lin, S. Das Sarma, and R. M. Nandkishore, Superconductor versus insulator in twisted bilayer graphene, *Phys. Rev. B* **100**, 115128 (2019).
- [8] F. Guinea and N. R. Walet, Electrostatic effects, band distortions, and superconductivity in twisted graphene bilayers, *Proc. Natl. Acad. Sci.* **115**, 13174 (2018).
- [9] B. Lian, Z. Wang, and B. A. Bernevig, Twisted Bilayer Graphene: A Phonon-Driven Superconductor, *Phys. Rev. Lett.* **122**, 257002 (2019).
- [10] S. Ray, J. Jung, and T. Das, Wannier pairs in superconducting twisted bilayer graphene and related systems, *Phys. Rev. B* **99**, 134515 (2019).
- [11] M. J. Calderón and E. Bascones, Correlated states in magic angle twisted bilayer graphene under the optical conductivity scrutiny, [arXiv:1912.09935](#).
- [12] Y. Saito, J. Ge, K. Watanabe, T. Taniguchi, and A. F. Young, Decoupling superconductivity and correlated insulators in twisted bilayer graphene, [arXiv:1911.13302](#).
- [13] P. Stepanov, I. Das, X. Lu, A. Fahimniya, K. Watanabe, T. Taniguchi, F. H. L. Koppens, J. Lischner, L. Levitov, and D. K. Efetov, The interplay of insulating and superconducting orders in magic-angle graphene bilayers, [arXiv:1911.09198](#).
- [14] J. Kang and O. Vafek, Strong Coupling Phases of Partially Filled Twisted Bilayer Graphene Narrow Bands, *Phys. Rev. Lett.* **122**, 246401 (2019).
- [15] G. E. Volovik, Graphite, graphene, and the flat band superconductivity, *JETP Lett.* **107**, 516 (2018).
- [16] H. C. Po, L. Zou, A. Vishwanath, and T. Senthil, Origin of Mott Insulating Behavior and Superconductivity in Twisted Bilayer Graphene, *Phys. Rev. X* **8**, 031089 (2018).
- [17] M. Ochi, M. Koshino, and K. Kuroki, Possible correlated insulating states in magic-angle twisted bilayer graphene under strongly competing interactions, *Phys. Rev. B* **98**, 081102(R) (2018).
- [18] J. González and T. Stauber, Kohn-Luttinger Superconductivity in Twisted Bilayer Graphene, *Phys. Rev. Lett.* **122**, 026801 (2019).
- [19] Y. Sherkunov and J. J. Betouras, Electronic phases in twisted bilayer graphene at magic angles as a result of Van Hove singularities and interactions, *Phys. Rev. B* **98**, 205151 (2018).
- [20] E. Laksono, J. N. Leaw, A. Reaves, M. Singh, X. Wang, S. Adam, and X. Gu, Singlet superconductivity enhanced by charge order in nested twisted bilayer graphene fermi surfaces, *Solid State Commun.* **282**, 38 (2018).
- [21] J. W. F. Venderbos and R. M. Fernandes, Correlations and electronic order in a two-orbital honeycomb lattice model for twisted bilayer graphene, *Phys. Rev. B* **98**, 245103 (2018).
- [22] S. Shallcross, S. Sharma, E. Kandelaki, and O. A. Pankratov, Electronic structure of turbostratic graphene, *Phys. Rev. B* **81**, 165105 (2010).
- [23] T. Salamon, A. Celi, R. W. Chhajlany, I. Frérot, M. Lewenstein, L. Tarruell, and D. Rakshit, Simulating twistronics without a twist, [arXiv:1912.12736](#).
- [24] D. Weckbecker, S. Shallcross, M. Fleischmann, N. Ray, S. Sharma, and O. Pankratov, Low-energy theory for the graphene twist bilayer, *Phys. Rev. B* **93**, 035452 (2016).
- [25] F. Rost, R. Gupta, M. Fleischmann, D. Weckbecker, N. Ray, J. Olivares, M. Vogl, S. Sharma, O. Pankratov, and S. Shallcross, Nonperturbative theory of effective Hamiltonians for deformations in two-dimensional materials: Moiré systems and dislocations, *Phys. Rev. B* **100**, 035101 (2019).
- [26] M. Vogl, O. Pankratov, and S. Shallcross, Semiclassics for matrix Hamiltonians: The gutzwiller trace formula with applications to graphene-type systems, *Phys. Rev. B* **96**, 035442 (2017).
- [27] Y. Cheng, C. Huang, H. Hong, Z. Zhao, and K. Liu, Emerging properties of two-dimensional twisted bilayer materials, *Chin. Phys. B* **28**, 107304 (2019).
- [28] K. Liu, L. Zhang, T. Cao, C. Jin, D. Qiu, Q. Zhou, A. Zettl, P. Yang, S. G. Louie, and F. Wang, Evolution of interlayer coupling in twisted molybdenum disulfide bilayers, *Nat. Commun.* **5**, 4966 (2014).
- [29] J.-Y. Wu, W.-P. Su, and G. Gumbs, Anomalous magnetotransport properties of bilayer phosphorene, *Sci. Rep.* **10**, 7674 (2020).
- [30] C. Shang, A. About, X. Zang, U. Schwingenschlogl, and A. Manchon, Artificial gauge fields and topological insulators in Moiré superlattices, [arXiv:1912.00447](#).
- [31] H. M. Abdullah, B. Van Duppen, M. Zarenia, H. Bahlouli, and F. M. Peeters, Quantum transport across van der waals domain walls in bilayer graphene, *J. Phys.: Condens. Matter* **29**, 425303 (2017).
- [32] Y. Xie, B. Lian, B. Jäck, X. Liu, C.-L. Chiu, K. Watanabe, T. Taniguchi, B. A. Bernevig, and A. Yazdani, Spectroscopic signatures of many-body correlations in magic-angle twisted bilayer graphene, *Nature (London)* **572**, 101 (2019).
- [33] P. A. Lee, N. Nagaosa, and X.-G. Wen, Doping a mott insulator: Physics of high-temperature superconductivity, *Rev. Mod. Phys.* **78**, 17 (2006).
- [34] Y. Cao, V. Fatemi, A. Demir, S. Fang, S. L. Tomarken, J. Y. Luo, J. D. Sanchez-Yamagishi, K. Watanabe, T. Taniguchi, E. Kaxiras, R. C. Ashoori, and P. Jarillo-Herrero, Correlated insulator behavior at half-filling in magic-angle graphene superlattices, *Nature (London)* **556**, 80 (2018).
- [35] Y. Zhang, K. Jiang, Z. Wang, and F. Zhang, Correlated insulating phases of twisted bilayer graphene at commensurate filling fractions: a hartree-fock study, [arXiv:2001.02476](#).
- [36] D. Wong, K. P. Nuckolls, M. Oh, B. Lian, Y. Xie, S. Jeon, K. Watanabe, T. Taniguchi, B. A. Bernevig, and A. Yazdani, Cascade of transitions between the correlated electronic states of magic-angle twisted bilayer graphene, [arXiv:1912.06145](#).

- [37] A. L. Sharpe, E. J. Fox, A. W. Barnard, J. Finney, K. Watanabe, T. Taniguchi, M. A. Kastner, and D. Goldhaber-Gordon, Emergent ferromagnetism near three-quarters filling in twisted bilayer graphene, *Science* **365**, 605 (2019).
- [38] K. Seo, V. N. Kotov, and B. Uchoa, Ferromagnetic Mott State in Twisted Graphene Bilayers at the Magic Angle, *Phys. Rev. Lett.* **122**, 246402 (2019).
- [39] R. Bistritzer and A. H. MacDonald, Moiré bands in twisted double-layer graphene, *Proc. Natl. Acad. Sci.* **108**, 12233 (2011).
- [40] K. Kim, A. DaSilva, S. Huang, B. Fallahzad, S. Larentis, T. Taniguchi, K. Watanabe, B. J. LeRoy, A. H. MacDonald, and E. Tutuc, Tunable Moiré bands and strong correlations in small-twist-angle bilayer graphene, *Proc. Natl. Acad. Sci.* **114**, 3364 (2017).
- [41] M. I. B. Utama, R. J. Koch, K. Lee, N. Leconte, H. Li, S. Zhao, L. Jiang, J. Zhu, K. Watanabe, T. Taniguchi, P. D. Ashby, A. Weber-Bargioni, A. Zettl, C. Jozwiak, J. Jung, E. Rotenberg, A. Bostwick, and F. Wang, Visualization of the flat electronic band in twisted bilayer graphene near the magic angle twist, [arXiv:1912.00587](https://arxiv.org/abs/1912.00587).
- [42] S. Carr, S. Fang, P. Jarillo-Herrero, and E. Kaxiras, Pressure dependence of the magic twist angle in graphene superlattices, *Phys. Rev. B* **98**, 085144 (2018).
- [43] B. L. Chittari, N. Leconte, S. Javvaji, and J. Jung, Pressure induced compression of flatbands in twisted bilayer graphene, *Electronic Structure* **1**, 015001 (2018).
- [44] M. Yankowitz, J. Jung, E. Laksono, N. Leconte, B. L. Chittari, K. Watanabe, T. Taniguchi, S. Adam, D. Graf, and C. R. Dean, Dynamic band-structure tuning of graphene Moiré superlattices with pressure, *Nature (London)* **557**, 404 (2018).
- [45] M. Vogl, M. Rodriguez-Vega, and G. A. Fiete, Floquet engineering of interlayer couplings: Tuning the magic angle of twisted bilayer graphene at the exit of a waveguide, [arXiv:2001.04416](https://arxiv.org/abs/2001.04416).
- [46] A. Polkovnikov, K. Sengupta, A. Silva, and M. Vengalattore, Colloquium: Nonequilibrium dynamics of closed interacting quantum systems, *Rev. Mod. Phys.* **83**, 863 (2011).
- [47] A. Eckardt, Colloquium: Atomic quantum gases in periodically driven optical lattices, *Rev. Mod. Phys.* **89**, 011004 (2017).
- [48] I. Bloch, J. Dalibard, and W. Zwerger, Many-body physics with ultracold gases, *Rev. Mod. Phys.* **80**, 885 (2008).
- [49] J. Dalibard, F. Gerbier, G. Juzeliūnas, and P. Öhberg, Colloquium: Artificial gauge potentials for neutral atoms, *Rev. Mod. Phys.* **83**, 1523 (2011).
- [50] D. N. Basov, R. D. Averitt, and D. Hsieh, Towards properties on demand in quantum materials, *Nat. Mater.* **16**, 1077 (2017).
- [51] J. Zhang and R. D. Averitt, Dynamics and control in complex transition metal oxides, *Annu. Rev. Mater. Res.* **44**, 19 (2014).
- [52] D. N. Basov, R. D. Averitt, D. van der Marel, M. Dressel, and K. Haule, Electrodynamics of correlated electron materials, *Rev. Mod. Phys.* **83**, 471 (2011).
- [53] C. Giannetti, M. Capone, D. Fausti, M. Fabrizio, F. Parmigiani, and D. Mihailovic, Ultrafast optical spectroscopy of strongly correlated materials and high-temperature superconductors: a non-equilibrium approach, *Adv. Phys.* **65**, 58 (2016).
- [54] M. Gandolfi, G. L. Celardo, F. Borgonovi, G. Ferrini, A. Avella, F. Banfi, and C. Giannetti, Emergent ultrafast phenomena in correlated oxides and heterostructures, *Phys. Scr.* **92**, 034004 (2017).
- [55] O. V. Kibis, Metal-insulator transition in graphene induced by circularly polarized photons, *Phys. Rev. B* **81**, 165433 (2010).
- [56] O. V. Kibis, S. Morina, K. Dini, and I. A. Shelykh, Magneto-electronic properties of graphene dressed by a high-frequency field, *Phys. Rev. B* **93**, 115420 (2016).
- [57] O. V. Kibis, K. Dini, I. V. Iorsh, and I. A. Shelykh, All-optical band engineering of gapped dirac materials, *Phys. Rev. B* **95**, 125401 (2017).
- [58] I. V. Iorsh, K. Dini, O. V. Kibis, and I. A. Shelykh, Optically induced lifshitz transition in bilayer graphene, *Phys. Rev. B* **96**, 155432 (2017).
- [59] R. Moessner and S. L. Sondhi, Equilibration and order in quantum Floquet matter, *Nat. Phys.* **13**, 424 (2017).
- [60] D. A. Abanin, W. De Roeck, and F. Huvneers, Exponentially Slow Heating in Periodically Driven Many-Body Systems, *Phys. Rev. Lett.* **115**, 256803 (2015).
- [61] D. A. Abanin, W. De Roeck, W. W. Ho, and F. Huvneers, Effective Hamiltonians, prethermalization, and slow energy absorption in periodically driven many-body systems, *Phys. Rev. B* **95**, 014112 (2017).
- [62] T. Mori, T. Kuwahara, and K. Saito, Rigorous Bound on Energy Absorption and Generic Relaxation in Periodically Driven Quantum Systems, *Phys. Rev. Lett.* **116**, 120401 (2016).
- [63] D. V. Else, B. Bauer, and C. Nayak, Prethermal Phases of Matter Protected by Time-Translation Symmetry, *Phys. Rev. X* **7**, 011026 (2017).
- [64] E. Canovi, M. Kollar, and M. Eckstein, Stroboscopic prethermalization in weakly interacting periodically driven systems, *Phys. Rev. E* **93**, 012130 (2016).
- [65] A. Eckardt and E. Anisimovas, High-frequency approximation for periodically driven quantum systems from a Floquet-space perspective, *New J. Phys.* **17**, 093039 (2015).
- [66] T. Mikami, S. Kitamura, K. Yasuda, N. Tsuji, T. Oka, and H. Aoki, Brillouin-Wigner theory for high-frequency expansion in periodically driven systems: Application to Floquet topological insulators, *Phys. Rev. B* **93**, 144307 (2016).
- [67] S. Blanes, F. Casas, J. A. Oteo, and J. Ros, The Magnus expansion and some of its applications, *Phys. Rep.* **470**, 151 (2009).
- [68] E. B. Fel'dman, On the convergence of the Magnus expansion for spin systems in periodic magnetic fields, *Phys. Lett. A* **104**, 479 (1984).
- [69] W. Magnus, On the exponential solution of differential equations for a linear operator, *Commun. Pure Appl. Math.* **7**, 649 (1954).
- [70] M. Bukov, L. D'Alessio, and A. Polkovnikov, Universal high-frequency behavior of periodically driven systems: From dynamical stabilization to Floquet engineering, *Adv. Phys.* **64**, 139 (2015).
- [71] S. Rahav, I. Gilary, and S. Fishman, Effective Hamiltonians for periodically driven systems, *Phys. Rev. A* **68**, 013820 (2003).
- [72] N. Goldman and J. Dalibard, Periodically Driven Quantum Systems: Effective Hamiltonians and Engineered Gauge Fields, *Phys. Rev. X* **4**, 031027 (2014).
- [73] A. P. Itin and M. I. Katsnelson, Effective Hamiltonians for Rapidly Driven Many-Body Lattice Systems: Induced

- Exchange Interactions and Density-Dependent Hoppings, *Phys. Rev. Lett.* **115**, 075301 (2015).
- [74] P. Mohan, R. Saxena, A. Kundu, and S. Rao, Brillouin-Wigner theory for Floquet topological phase transitions in spin-orbit-coupled materials, *Phys. Rev. B* **94**, 235419 (2016).
- [75] M. Bukov, M. Kolodrubetz, and A. Polkovnikov, Schrieffer-Wolff Transformation for Periodically Driven Systems: Strongly Correlated Systems with Artificial Gauge Fields, *Phys. Rev. Lett.* **116**, 125301 (2016).
- [76] M. M. Maricq, Application of average Hamiltonian theory to the NMR of solids, *Phys. Rev. B* **25**, 6622 (1982).
- [77] M. Vogl, P. Laurell, A. D. Barr, and G. A. Fiete, Flow Equation Approach to Periodically Driven Quantum Systems, *Phys. Rev. X* **9**, 021037 (2019).
- [78] M. Vogl, P. Laurell, A. D. Barr, and G. A. Fiete, Analog of Hamilton-Jacobi theory for the time-evolution operator, *Phys. Rev. A* **100**, 012132 (2019).
- [79] M. Vogl, M. Rodriguez-Vega, and G. A. Fiete, Effective Floquet Hamiltonian in the low-frequency regime, *Phys. Rev. B* **101**, 024303 (2020).
- [80] M. Rodriguez-Vega, M. Lentz, and B. Seradjeh, Floquet perturbation theory: Formalism and application to low-frequency limit, *New J. Phys.* **20**, 093022 (2018).
- [81] H. Martiskainen and N. Moiseyev, Perturbation theory for quasienergy Floquet solutions in the low-frequency regime of the oscillating electric field, *Phys. Rev. A* **91**, 023416 (2015).
- [82] G. Rigolin, G. Ortiz, and V. H. Ponce, Beyond the quantum adiabatic approximation: Adiabatic perturbation theory, *Phys. Rev. A* **78**, 052508 (2008).
- [83] M. Weinberg, C. Ölschläger, C. Sträter, S. Prella, A. Eckardt, K. Sengstock, and J. Simonet, Multiphoton interband excitations of quantum gases in driven optical lattices, *Phys. Rev. A* **92**, 043621 (2015).
- [84] J.-M. Li, K.-H. He, Z.-F. Shi, H.-Y. Gao, and Y.-M. Jiang, Synthesis, crystal structures, and thermal and spectroscopic properties of two cd(II) metal-organic frameworks with a versatile ligand, *Z. Naturforsch. B* **71**, 909 (2016).
- [85] A. Verdeny, A. Mielke, and F. Mintert, Accurate Effective Hamiltonians via Unitary Flow in Floquet Space, *Phys. Rev. Lett.* **111**, 175301 (2013).
- [86] J. C. Sandoval-Santana, V. G. Ibarra-Sierra, J. L. Cardoso, A. Kunold, P. Roman-Taboada, and G. Naumis, Method for finding the exact effective Hamiltonian of time-driven quantum systems, *Ann. Phys.* **531**, 1900035 (2019).
- [87] T. Oka and H. Aoki, Photovoltaic Hall effect in graphene, *Phys. Rev. B* **79**, 081406 (2009).
- [88] J. W. McIver, B. Schulte, F.-U. Stein, T. Matsuyama, G. Jotzu, G. Meier, and A. Cavalleri, Light-induced anomalous Hall effect in graphene, *Nat. Phys.* **16**, 38 (2020).
- [89] M. S. Rudner, N. H. Lindner, E. Berg, and M. Levin, Anomalous Edge States and the Bulk-Edge Correspondence for Periodically Driven Two-Dimensional Systems, *Phys. Rev. X* **3**, 031005 (2013).
- [90] N. H. Lindner, G. Refael, and V. Galitski, Floquet topological insulator in semiconductor quantum wells, *Nat. Phys.* **7**, 490 (2011).
- [91] Q.-J. Tong, J.-H. An, J. Gong, H.-G. Luo, and C. H. Oh, Generating many majorana modes via periodic driving: A superconductor model, *Phys. Rev. B* **87**, 201109 (2013).
- [92] M. Thakurathi, A. A. Patel, D. Sen, and A. Dutta, Floquet generation of majorana end modes and topological invariants, *Phys. Rev. B* **88**, 155133 (2013).
- [93] A. Kundu and B. Seradjeh, Transport Signatures of Floquet Majorana Fermions in Driven Topological Superconductors, *Phys. Rev. Lett.* **111**, 136402 (2013).
- [94] M. C. Rechtsman, J. M. Zeuner, Y. Plotnik, Y. Lumer, D. Podolsky, F. Dreisow, S. Nolte, M. Segev, and A. Szameit, Photonic Floquet topological insulators, *Nature (London)* **496**, 196 (2013).
- [95] L. JianT. Kitagawa, J. Alicea, A. R. Akhmerov, D. Pekker, G. Refael, J. I. Cirac, E. Demler, M. D. Lukin, and P. Zoller, Majorana Fermions in Equilibrium and in Driven Cold-Atom Quantum Wires, *Phys. Rev. Lett.* **106**, 220402 (2011).
- [96] Z. Gu, H. A. Fertig, D. P. Arovas, and A. Auerbach, Floquet Spectrum and Transport through an Irradiated Graphene Ribbon, *Phys. Rev. Lett.* **107**, 216601 (2011).
- [97] P. M. Perez-Piskunow, G. Usaj, C. A. Balseiro, and L. E. F. Foa Torres, Floquet chiral edge states in graphene, *Phys. Rev. B* **89**, 121401 (2014).
- [98] G. Usaj, P. M. Perez-Piskunow, L. E. F. Foa Torres, and C. A. Balseiro, Irradiated graphene as a tunable Floquet topological insulator, *Phys. Rev. B* **90**, 115423 (2014).
- [99] P. M. Perez-Piskunow, L. E. F. Foa Torres, and G. Usaj, Hierarchy of Floquet gaps and edge states for driven honeycomb lattices, *Phys. Rev. A* **91**, 043625 (2015).
- [100] H. L. Calvo, L. E. F. Foa Torres, P. M. Perez-Piskunow, C. A. Balseiro, and G. Usaj, Floquet interface states in illuminated three-dimensional topological insulators, *Phys. Rev. B* **91**, 241404 (2015).
- [101] B. Mukherjee, P. Mohan, D. Sen, and K. Sengupta, Low-frequency phase diagram of irradiated graphene and a periodically driven spin- $\frac{1}{2}$ xy chain, *Phys. Rev. B* **97**, 205415 (2018).
- [102] I. Esin, M. S. Rudner, G. Refael, and N. H. Lindner, Quantized transport and steady states of Floquet topological insulators, *Phys. Rev. B* **97**, 245401 (2018).
- [103] M. S. Rudner and N. H. Lindner, Floquet topological insulators: From band structure engineering to novel non-equilibrium quantum phenomena, [arXiv:1909.02008](https://arxiv.org/abs/1909.02008).
- [104] H. Deghani, T. Oka, and A. Mitra, Out-of-equilibrium electrons and the hall conductance of a Floquet topological insulator, *Phys. Rev. B* **91**, 155422 (2015).
- [105] H. Deghani and A. Mitra, Optical hall conductivity of a Floquet topological insulator, *Phys. Rev. B* **92**, 165111 (2015).
- [106] H. Deghani and A. Mitra, Occupation probabilities and current densities of bulk and edge states of a Floquet topological insulator, *Phys. Rev. B* **93**, 205437 (2016).
- [107] J. Klinovaja, P. Stano, and D. Loss, Topological Floquet Phases in Driven Coupled Rashba Nanowires, *Phys. Rev. Lett.* **116**, 176401 (2016).
- [108] G. E. Topp, G. Jotzu, J. W. McIver, L. Xian, A. Rubio, and M. A. Sentef, Topological Floquet engineering of twisted bilayer graphene, *Phys. Rev. Research* **1**, 023031 (2019).
- [109] Y. Li, H. A. Fertig, and B. Seradjeh, Floquet-engineered topological flat bands in irradiated twisted bilayer graphene, [arXiv:1910.04711](https://arxiv.org/abs/1910.04711).

- [110] O. Katz, G. Refael, and N. H. Lindner, Optically induced flat bands in twisted bilayer graphene, [arXiv:1910.13510](#).
- [111] E. Perfetto and G. Stefanucci, Some exact properties of the nonequilibrium response function for transient photoabsorption, *Phys. Rev. A* **91**, 033416 (2015).
- [112] U. De Giovannini and H. Hübener, Floquet analysis of excitations in materials, *J. Phys.: Materials* **3**, 012001 (2019).
- [113] M. Fleischmann, R. Gupta, F. Wullschläger, S. Theil, D. Weckbecker, V. Meded, S. Sharma, B. Meyer, and S. Shallcross, Perfect and controllable nesting in the small angle twist bilayer graphene, *Nano Lett.* **20**, 971 (2020).
- [114] M. Fleischmann, R. Gupta, S. Sharma, and S. Shallcross, Moiré quantum well states in tiny angle two dimensional semi-conductors, [arXiv:1901.04679](#).
- [115] M. Xie and A. H. MacDonald, Nature of the Correlated Insulator States in Twisted Bilayer Graphene, *Phys. Rev. Lett.* **124**, 097601 (2020).
- [116] N. N. T. Nam and M. Koshino, Lattice relaxation and energy band modulation in twisted bilayer graphene, *Phys. Rev. B* **96**, 075311 (2017).
- [117] F. Guinea and N. R. Walet, Continuum models for twisted bilayer graphene: Effect of lattice deformation and hopping parameters, *Phys. Rev. B* **99**, 205134 (2019).
- [118] L. Balents, General continuum model for twisted bilayer graphene and arbitrary smooth deformations, *SciPost Phys.* **7**, 48 (2019).
- [119] K. Hejazi, C. Liu, H. Shapourian, X. Chen, and L. Balents, Multiple topological transitions in twisted bilayer graphene near the first magic angle, *Phys. Rev. B* **99**, 035111 (2019).
- [120] A. G. Grushin, Á. Gómez-León, and T. Neupert, Floquet Fractional Chern Insulators, *Phys. Rev. Lett.* **112**, 156801 (2014).
- [121] Y. Zhang, T.-T. Tang, C. Girit, Z. Hao, M. C. Martin, A. Zettl, M. F. Crommie, Y. R. Shen, and F. Wang, Direct observation of a widely tunable bandgap in bilayer graphene, *Nature (London)* **459**, 820 (2009).
- [122] K. F. Mak, C. H. Lui, J. Shan, and T. F. Heinz, Observation of an Electric-Field-Induced Band Gap in Bilayer Graphene by Infrared Spectroscopy, *Phys. Rev. Lett.* **102**, 256405 (2009).
- [123] Z. Qiao, J. Jung, Q. Niu, and A. H. MacDonald, Electronic highways in bilayer graphene, *Nano Lett.* **11**, 3453 (2011).
- [124] I. Martin, Y. M. Blanter, and A. F. Morpurgo, Topological Confinement in Bilayer Graphene, *Phys. Rev. Lett.* **100**, 036804 (2008).
- [125] J. S. Alden, A. W. Tsen, P. Y. Huang, R. Hovden, L. Brown, J. Park, D. A. Muller, and P. L. McEuen, Strain solitons and topological defects in bilayer graphene, *Proc. Natl. Acad. Sci.* **110**, 11256 (2013).
- [126] P. San-Jose and E. Prada, Helical networks in twisted bilayer graphene under interlayer bias, *Phys. Rev. B* **88**, 121408 (2013).